INTERNATIONAL JOURNAL FOR NUMERICAL METHODS IN FLUIDS, VOL. 21, 993–1005 (1995)

NUMERICAL ANALYSIS OF 2D VORTEX-INDUCED OSCILLATIONS OF A CIRCULAR CYLINDER

R. WEI, A. SEKINE AND M. SHIMURA

Technical Research Institute of Maeda Corporation, Tokyo, Japan

SUMMARY

In this paper a finite element version of the direct Laplacian method is applied to flows around an oscillating body, using the arbitrary Langrangian–Eulerian (ALE) formulation for the partial domain around the body. This numerical calculation has been successfully conducted for vortex-induced, cross-flow oscillations of a circular cylinder under the same conditions as for Anagnostopoulos and Bearman's experiment (*J. Fluids Struct.*, **6**, 39–50 (1992)), in which the Reynolds number ranged between 90 and 150, a regime where the vortex street is fully laminar. The numerical calculation results have been compared with the experimental data in order to check the calculational accuracy.

KEY WORDS: FEM analysis; ALE method; vortex-induced oscillation

1. INTRODUCTION

The problems of fluid-structure interaction attracts much attention in civil and building engineering. The affect of a fluid (e.g. wind) on a structure is normally considered as a fluctuating or average wind pressure acting on the surface of the structure when undertaking a structural design. In recent years, with the development of construction technology, many large structures such as super-high-rise buildings, long-span bridges and large domes with light roofs have been built or are being planned. These large structures can no longer be treated as rigid bodies, because their natural frequencies are comparatively low. If their natural frequencies are close to vortex-shedding frequencies and the vibration-damping coefficient is sufficiently small, self-excited vibrations may be induced. Furthermore, large amplitudes of vibration may influence the surrounding flow pattern and consequently lead to more serious non-linear interaction between the flow and the structure motion. Then structural damage may occur. Therefore it is necessary to study this phenomenon.

The present paper is aimed at solving such a fluid–structure interaction problem computationally, where the structure is often idealized as a rigid body supported by elastic springs. The key point in solving such a problem is the treatment of the moving interface between the fluid and the rigid body. We have developed a finite element method for interaction problems of viscous incompressible fluid flows and motion of an elastically mounted rigid cylinder by using the ALE method. The present analysis method features (i) a semi-implicit scheme utilizing the finite element method, (ii) a direct Laplacian approximation for the pressure equation and (iii) an efficient application of the ALE method for the moving boundary. A numerical calculation has been carried out to simulate the vortex-induced vibrations of a circular cylinder under the same conditions as for Anagnostopoulos and Bearman's[1] experiment.

In the branch of CFD employing finite elements, the first approaches to treating the moving boundary interface were taken in the 1970s. Belytschko and Kennedy[2] applied calculations of the

CCC 0271–2091/95/100993–13

Received 6 June 1994
Revised 10 November 1994

vibration of pipes in nuclear reactors for the first time; Donea *et al.*[3] also worked on the same problems. However, in those calculations only the Lagrangian method was applicable to describe the momentum equation, so there were limitations in solving problems involving large deformations of the moving boundary. In the 1980s Hughes *et al.*[4] Lin *et al.*[5] and Ramaswany and Kawahara[6] presented the arbitrary Lagrangian–Eulerian (ALE) finite element method. (In fact, the ALE method was first mentioned by Hirt *et al.*[7] based on a formulation of the finite difference method.) In the early 1990s Mittal and Tezduyar[8] gave some explanations of the causes of 'lock-in' and 'hysteresis'.

This paper is structured as follows. In Section 2 the basic ALE concept and how to apply the ALE method to the Navier–Stokes (N–S) equation are briefly described. In Section 3 the computational procedure derived from the direct Laplacian method is presented. In Section 4 a numerical analysis of vortex-induced cylinder oscillations is conducted to compare with the reported experimental results. Section 5 contains some concluding remarks.

2. ALE CONCEPT AND APPLICATION TO N–S EQUATION

The governing equations for time-dependent incompressible viscous flow consist of the Navier–Stokes equation and the continuity equation, which are written as follows in non-dimensional form:

$$\rho\left(\frac{\partial u_i}{\partial t} + u_j \frac{\partial u_i}{\partial x_j}\right) = \rho b_i + \frac{\partial \tau_{ij}}{\partial x_j}, \tag{1}$$

$$\frac{\partial u_i}{\partial x_i} = 0. \tag{2}$$

Equation (1) represents momentum conservation and equation (2) is the statement of mass conservation. Here τ_{ij} is the stress tensor, which can be defined as

$$\tau_{ij} = -P\delta_{ij} + \mu\left(\frac{\partial u_i}{\partial x_j} + \frac{\partial u_j}{\partial x_i}\right). \tag{3}$$

Equations (1)–(3) are valid only when the fluid is under the incompressibility constraint and the density is constant. Here u_i is the velocity vector in the i-direction, t is the time, b_i is the unit body force vector in the i-direction, ρ is the fluid density, P is the pressure, δ_{ij} is the Kronecker symbol and μ is the coefficient of material viscosity.

Equation (1) is only applicable for a fixed Eulerian co-ordinate x and cannot be utilized in the moving boundary problem. Here we can assume that there exists a moving co-ordinate system X which is deformed with the moving boundary under a certain rule. In such a co-ordinate system as shown in Figure 1, if we assume that a particle flows from point A to point B with a movement of Δx while the co-ordinate X moves from point A to point C with a movement of Δy in a very short time Δt, then

$$\Delta x - \Delta y = (U - V)\Delta t, \tag{4}$$

where U denotes the velocity of the particle and V denotes the velocity of the moving co-ordinate X. Observing the motion of point B from point C, the differentiation of a function $f(x, t)$ can be defined as

$$\mathrm{D}f = f(x, t) + \Delta f(x, t) = f(x + (\Delta x - \Delta y), t + \Delta t). \tag{5}$$

Using a Taylor series expansion in time to second-order accuracy gives

$$\mathrm{D}f \approx f(x, t) + \Delta f(x, t) = f(x, t) + \frac{\mathrm{d}f(x, t)}{\mathrm{dx}}(\Delta x - \Delta y) + \frac{\mathrm{d}f(x, t)}{\mathrm{dt}}\Delta t + O(\Delta t^2). \tag{6}$$

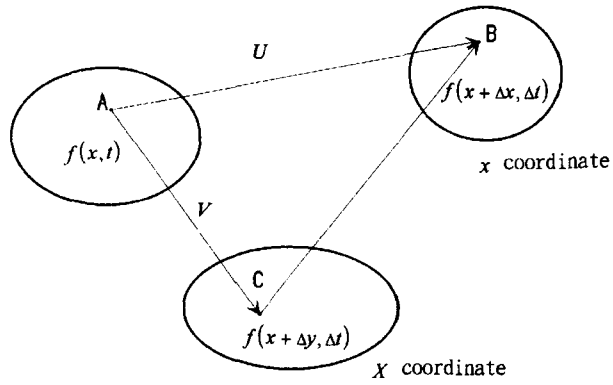

Figure 1. Co-ordinate system for arbitrary Lagrangian–Eulerian description

When Δt is near zero, by introducing equation (4) into (6), the following equation can be derived:

$$\frac{\mathrm{D}f}{\mathrm{D}t} \approx \left.\frac{\mathrm{d}f(x,t)}{\mathrm{d}t}\right|_X + \frac{\mathrm{d}f(x,t)}{\mathrm{d}x}(U-V). \tag{7}$$

From (7) we know that in the ALE description the value of U–V influences the convection term of the N–S equation. Since the stress tensor, body force vector and continuity equation have no relation with time differentiation, they do not change in the ALE description. In this case equation (7) is equivalent to the Euler co-ordinate description when $V=0$ and to the Lagrangian co-ordinate description when $V=U$. This is the reason why this method is called the ALE method. Finally, the basic flow field equations used with the ALE method can be written as

$$\rho\left(\frac{\partial u_i}{\partial t} + (u_j - v_j)\frac{\partial u_i}{\partial x_j}\right) = \rho b_i + \frac{\partial \tau_{ij}}{\partial x_j}, \tag{8}$$

$$\frac{\partial u_i}{\partial x_i} = 0 \tag{9}$$

and then how to apply the movement rule to the nodes is the key point.[9]

3. COMPUTATIONAL PRINCIPLES

The basic equations for time-dependent incompressible viscous flow consists of the Navier–Stokes equation and the continuity equation, which are written as follows in non-dimensional form:

$$\frac{\partial U}{\partial t} + (U-V)(U\cdot\nabla) + \nabla P - \frac{1}{Re}\nabla^2 U = 0, \tag{10}$$

$$\nabla \cdot U = 0. \tag{11}$$

The kinetic equation for the structural component is the well-known expression

$$M\ddot{x} + C\dot{x} + Kx = f, \tag{12}$$

where x and f are the displacement of the structure and the fluid force respectively and M, C and K are the mass, damping and stiffness matrices respectively. Since it is very difficult and laborious to solve

these equations fully coupled, for simplicity and efficiency of calculation the fractional step method is applied to the interaction problem. In Section 3.1 we will discuss the fractional step method briefly.

3.1. *Fractional step method*

Applying the forward Euler scheme to the time derivative term, i.e. $\partial U/\partial t \approx (U^{m+1} - U^m)/\Delta t$, and approximating the pressure as $P \approx P^{m+1}$, equation (10) is rewritten in the following form, where P is a scalar and U is a vector;

$$\frac{U^{m+1} - U^m}{\Delta t} + (U^m - V^m)(U^m \cdot \nabla) + \nabla P^{m+1} - \frac{1}{Re}\nabla^2 U^m = 0. \tag{13}$$

Taking the divergence of both sides of (13) and substituting the continuity condition $\nabla \cdot U^{m+1} = 0$, the pressure Poisson equation can be obtained as

$$\nabla^2 P^{m+1} = \frac{1}{\Delta t}\nabla \cdot \tilde{U}, \tag{14}$$

where

$$\tilde{U} = U^m + \Delta t\left(\frac{1}{Re}\nabla^2 U^m - (U^m - V^m)(U^m \cdot \nabla)\right). \tag{15}$$

Here $\tilde{U}$ is an intermediate variable and plays the role of predictor. The gradient P^{m+1} is the corrector for U^{m+1}.

3.2. *Finite element method*

The finite element method is used for the spatial discretization of the equations. The weighted residual equations of (15), (14) and (13) are formulated respectively as

$$\int_\Omega \tilde{U}^* U \mathrm{d}\Omega = \int_\Omega \tilde{U}^* U^m \mathrm{d}\Omega + \Delta t \times \left(\frac{1}{Re}\int_\Gamma \tilde{U}^* \nabla U^m \mathrm{d}\Gamma - \frac{1}{Re}\int_\Omega \nabla \tilde{U}^* \nabla U^m \mathrm{d}\Omega - \int_\Omega \tilde{U}^*(U^m - V^m) \cdot \nabla U^m \mathrm{d}\Omega\right), \tag{16}$$

$$\int_\Omega \nabla P^* P^{m+1} \mathrm{d}\Omega = \int_\Gamma P^* \nabla P^{m+1} \mathrm{d}\Gamma - \frac{1}{\Delta t}\int_\Omega P^* \nabla \cdot \tilde{U} \mathrm{d}\Omega, \tag{17}$$

$$\int_\Omega U^* U^{m+1} \mathrm{d}\Omega = \int_\Omega U^* \tilde{U} \mathrm{d}\,\Omega - \Delta t \int_\Omega U^* \nabla P^{m+1} \mathrm{d}\Omega, \tag{18}$$

where $\tilde{U}^*$, U^* and P^* are the weighting functions for the intermediate variable, primitive velocity and pressure respectively. The Laplacian terms of both velocity and pressure are decomposed by the formula for integration by parts. The standard Galerkin method is employed for the discretization of the basic equations. The interpolation and weighting functions are defined as

$$\tilde{U} = [N]\{\tilde{U}\}, \tag{19}$$

$$\tilde{U}^* = [N]\{\tilde{U}^*\}, \tag{20}$$

$$U = [N]\{U\}, \tag{21}$$

$$U^* = [N]\{U^*\}, \tag{22}$$

$$P = [N]\{P\}, \tag{23}$$

$$P^* = [N]\{P^*\}, \tag{24}$$

where N is the interpolation function. In this paper the bilinear function based on the four-node quadrilateral element is employed for all variables. The present fractional step method does not require any stabilizing technique. At the same time the constraint of the LBB condition is avoided by considering the pressure Dirichlet condition in the Poisson equation

The finite element equations can be formulated as

$$\bar{M}\tilde{U} = \bar{M}U^m + \Delta t\left(\frac{1}{Re}(C - S)U^m - A(U^m)(U^m - V^m)\right), \tag{25}$$

$$SP^{m+1} = CP^{m+1} - \frac{1}{\Delta t}H\tilde{U}, \tag{26}$$

$$\bar{M}U^{m+1} = \bar{M}\tilde{U} - \Delta t HP^{m+1}, \tag{27}$$

where

$$\bar{M} = \int_\Omega N^{\mathrm{T}} N \mathrm{d}\Omega, \tag{28}$$

$$S = \int_\Omega \nabla N^{\mathrm{T}} \nabla N \mathrm{d}\Omega, \tag{29}$$

$$C = \int_\Gamma N^{\mathrm{T}} \nabla N \mathrm{d}\Gamma, \tag{30}$$

$$A = \int_\Omega N^{\mathrm{T}} N \cdot \nabla N \mathrm{d}\Omega, \tag{31}$$

$$H = \int_\Omega N^{\mathrm{T}} \nabla N \mathrm{d}\Omega. \tag{32}$$

For the sake of calculational efficiency the lumped mass matrix is used instead of the consistent mass matrix in (25) and (27).

3.3. *Boundary condition for pressure and Shimura–Kawahara (S–K) scheme*

Equation (26) needs an appropriate Dirichlet boundary condition to be solved in algebraic terms. The treatment is described as follows.

The boundary condition for pressure is derived from the following equations on Γ, where $\Gamma = \partial\Omega$ and $\Gamma = \Gamma_1 \cup \Gamma_2 \cup \Gamma_3$:

$$\frac{\partial P^{m+1}}{\partial n} = \frac{1}{Re}\left(\frac{\partial^2 U_n^m}{\partial n^2} + \frac{\partial^2 U_n^m}{\partial \tau^2}\right) - \left(U_n^m \frac{\partial U_n}{\partial n} + U_\tau^m \frac{\partial U_n}{\partial \tau}\right) - \frac{U_n^{m+1} - U_n^m}{\Delta t}, \tag{33}$$

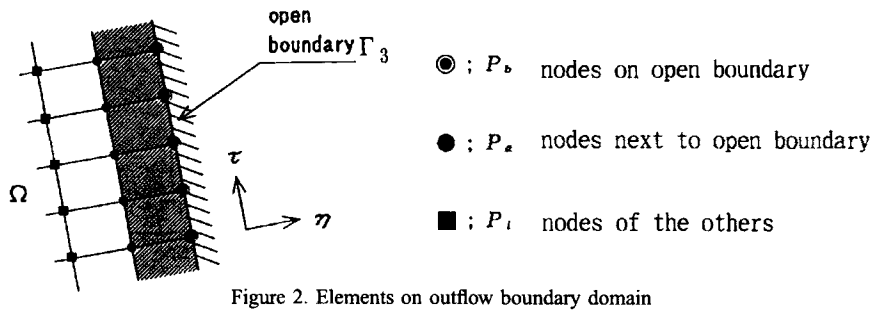

Figure 2. Elements on outflow boundary domain

$$\frac{\partial P^{m+1}}{\partial \tau} = \frac{1}{Re}\left(\frac{\partial^2 U_\tau^m}{\partial n^2} + \frac{\partial^2 U_\tau^m}{\partial \tau^2}\right) - \left(U_n^m \frac{\partial U_\tau}{\partial n} + U_\tau^m \frac{\partial U_\tau}{\partial \tau}\right) - \frac{U_\tau^{m+1} - U_\tau^m}{\Delta t}, \tag{34}$$

$$\frac{\partial U_n^{m+1}}{\partial n} + \frac{\partial U_\tau^{m+1}}{\partial \tau} = 0. \tag{35}$$

Here the velocity on Γ_1 (inlet) is given, the velocity on Γ_2 (wall) is zero and the velocity on Γ_3 (outlet) is unknown.

These equations are obtained by normal and tangential projections of (10) and (11) onto Γ. The coordinate system is shown in Figure 2. If the boundary condition for pressure is considered, the normal gradient term of pressure can be evaluated via (33), because the velocities U^{m+1} and U^m are given on Γ_1 and Γ_2. However, in general time-dependent problems neither the pressure gradient nor the pressure itself on the open boundary can be prescribed, because U^{m+1} on Γ_3 is unknown. Therefore a new approximation method to calculate the pressure on Γ_3 by using a similar procedure as for the inner domain of Ω is necessary and is proposed in the following manner.

It is very important to focus on the boundary condition of Navier–Stokes problems, especially in outflow or flow-through problems. Many researchers who are experienced in the practical computation of outflow problems know the significance of the open boundary condition in the location of the computational boundary.

Generally the boundary of the domain being analysed is called an open boundary and can be classified into inlet, wall and outflow boundaries. The inlet boundary Γ_1 is prescribed for the inflow velocity according to the analysis problem. The wall boundary Γ_2 is a no-slip boundary and this condition is generally defined as $U=0$. However, the outflow boundary Γ_3 cannot be defined so simply. If only flow velocity and pressure values are utilized as constant on Γ_3 throughout the calculation, the calculational results may be affected seriously and divergence may occur. In analysis methods not using the pressure Poisson equation, the traction-free condition is usually used as the outflow natural boundary condition. However, in the fractional step method, if the Dirichlet boundary condition for pressure is not imposed when solving the pressure Poisson equation (26), this calculation will have no algebraic solution. Furthermore, such boundary conditions should be regarded as additional but cannot be contradictory to the boundary conditions of the whole fluid domain.

Several years ago Shimura and Kawahara[10] proposed a generalized scheme for the treatment of the outflow boundary condition of the time-dependent N–S problem in the case of using the pressure Poisson equation. The traditional finite element solutions have a traction-free condition or an infinite condition on the outflow boundary. However, in a practical computation of the time-dependent problem it is impossible to prescribe the boundary condition on the computational boundary. It is necessary for the boundary to be treated similarly to the inner domain. Generally the best approach is to use the time-dependent boundary condition which is derived from the basic equations.

This idea is described and shown in Figure 2. Considering the open boundary domain which consists of the elements adjacent to the computational boundary, the same algebraic formulation as (14) is used in order to solve the boundary values P_b on the computational boundary, where the velocity field is known. In this scheme the pressure Poisson equation is calculated in two steps. In the first step, equation (36), the pressure values P_a assumed to be given on the inner-side nodes are utilised as the Dirichlet boundary condition (DBC) to solve P_b, because the pressure distribution on the inner-side nodes will be the best approximation for the computational boundary. In the second step, equation (37), the boundary pressure P_b is used for the DBC to solve the whole domain. In this way the pressure P_a on the inner side of the open boundary domain is automatically corrected during the second step when the pressure distribution on the whole domain is calculated. Only the initial values of pressure are needed for the pressure Poisson equation and the pressure distribution on the computational boundary is varied for each time step according to the velocity field.

$$\text{Step 1} \quad \begin{pmatrix} & \\ & S_b \end{pmatrix} \begin{Bmatrix} P_i^m \\ P_a^m \\ P_b \end{Bmatrix} = \begin{Bmatrix} f^m \\ \end{Bmatrix}. \tag{36}$$

$$\text{Step 2} \quad \begin{pmatrix} \\ S_{i+a} \\ \end{pmatrix} \begin{Bmatrix} P_i^{m+1} \\ P_a^{m+1} \\ P_b \end{Bmatrix} = \begin{Bmatrix} f^m \\ \end{Bmatrix}. \tag{37}$$

Remark. Equation (26) can be rewritten as

$$\begin{pmatrix} \\ S \\ \end{pmatrix} \begin{Bmatrix} P_i \\ P_a \\ P_b \end{Bmatrix} = \begin{Bmatrix} f \\ \end{Bmatrix},$$

in which the coefficient matrix S is reduced into S_b and S_{i+a} as follows during the calculation of the pressure Poisson equation:

$$\begin{pmatrix} \\ S \\ \end{pmatrix} = \begin{pmatrix} & \\ & S_b \end{pmatrix} + \begin{pmatrix} \\ S_{i+a} \\ \end{pmatrix}.$$

4. ANALYSIS OF VORTEX-INDUCED CYLINDER OSCILLATIONS

4.1. Calculation procedure

Many authors have applied the ALE method in the whole fluid field. This means that the finite element meshes of the whole domain have to be remeshed every time step and the calculation of the finite element matrices has to be repeated every time step, so the computational efficiency is poor. Therefore Shimura and Zienkiewicz[11] proposed the idea of applying the ALE method in a partial domain around the rigid body. The fluid field far from the rigid body is given a Eulerian description and the meshes in this domain are fixed through all time steps. Thus the remeshing domain is shrunk

and the calculational efficiency is significantly improved. However, determining the appropriate ALE domain depends on the displacement response of the rigid body. An ALE domain of insufficient area may result in projection errors. It may take some time to define a proper domain after repeated trial and error.

Figure 3 shows the analysis model. Defining a proper analysis domain before starting a numerical flow analysis can save on computing costs and make the computing performance more efficient while keeping the numerical results accurate. In the analysis of a fluid around a rigid body the fluid force acting on the body is influenced by the length in front, at the side and at the rear of the body. Too narrow domains may produce blockage phenomena as in wind tunnel tests. In our experience at least six times the body's width in the upstream and at both sides and eight times in the downstream are necessary.

The calculation procedure of the present method can be depicted as in Figure 4. Initial conditions and boundary values of the velocity field are given for each problem, but an impulsive start is usually imposed in the case of time-dependent problems. In the present calculation, four-node isoparametric bilinear elements were adopted for all variables. The next step is the forward reduction of the Laplacian matrix which is stored in skyline form.

In the time step loop the fluid force acting on the structure is first calculated, then the displacement of the structure can be solved from the kinetic equation via the usual scheme. In this calculation the linear acceleration method was used for the one-degree-of-freedom (Y) problem. If the structure is not rigid, it is easy to solve the deformation as a multiple-degree-of-freedom problem. Figure 5 shows the schematic description of the displacement of the structure. After calculating the structural displacement, the Lagrangian velocity V for each node in the ALE domain (points 4–6) can be obtained by linearization between the structure (points 7–9) and the Eulerian node (points 1–3), which is the interface of the Eulerian and Lagrangian domains. According to the new location of nodes, remeshing is implemented in the ALE domain. The intermediate variable can be calculated on the basis of the new mesh and the structural boundary condition $U = V$. Therefore the convection term vanishes on the surface of the structure. The next calculation is that of pressure values on the outflow boundary using the Poisson equation. Finally, the pressure field of the whole domain is obtained by backward substitution in the Poisson equation for the whole domain and the new velocity field is calculated using the momentum equation.

In the present scheme, because the pressure distribution on the computational boundary is automatically calculated, a Dirichlet boundary condition is necessary only for the velocity field.

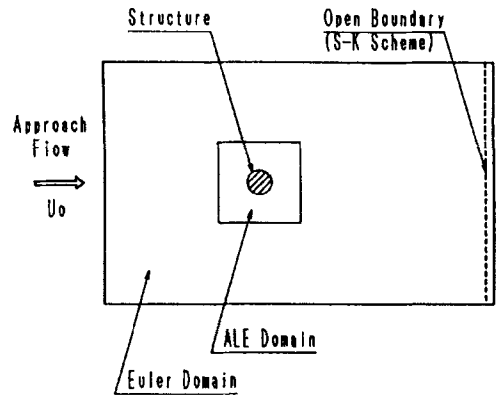

Figure 3. Analysis model

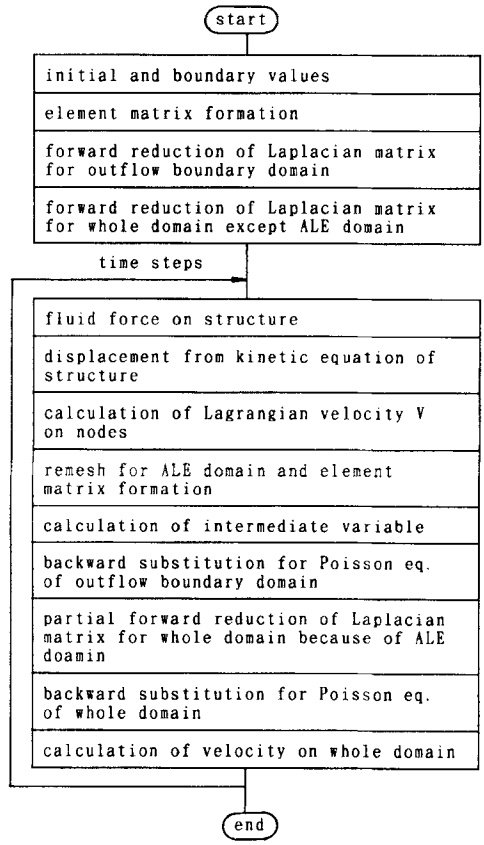

Figure 4. Calculation procedure

The time increment of the present method obeys the stability restriction

$$\Delta t \leqslant \frac{\Delta x}{2v/\Delta x + u}, \tag{38}$$

where Δx and v are the mesh size and the kinetic viscosity respectively.

In the analysis of the vortex excitation problem we have to estimate the drag and lift forces which induce the movement of the structure. In order to demonstrate the validity of the present method, a

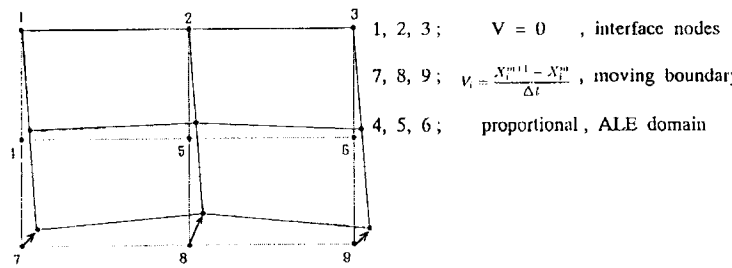

Figure 5. Description of structural displacement

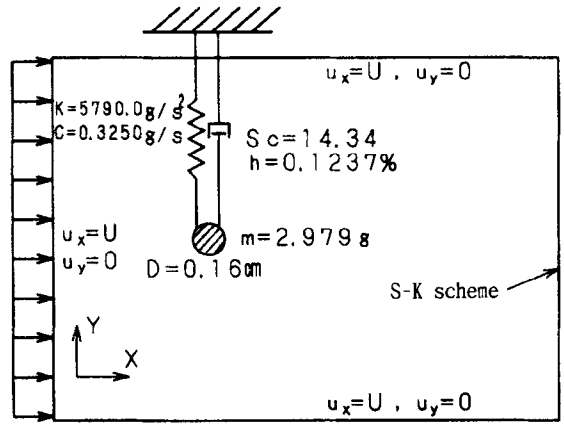

Figure 6. Conditions for analysis

vortex-induced oscillation analysis for a circular cylinder was implemented in the case of a resonance condition where the vortex separation period is equal to the natural oscillation period of the cylinder, which was measured in Anagnostopoulos and Bearman's[1] experiment.

The drag and lift force coefficients are obtained by the equations

$$f_x = \frac{(1/A)\oint n_x \tau_x \mathrm{d}s}{\rho_0 V_0^2/2}, \qquad f_y = \frac{(1/A)\oint n_y \tau_y \mathrm{d}s}{\rho_0 V_0^2/2},$$

where A is the representative area, n_x and n_y are the normal vector components, $\rho_0 V_0^2/2$ is the dynamic pressure at the inlet and f_x and f_y are the components of the force term in (12).

4.2. Numerical results

Anagnostopoulos and Bearman[1] conducted a series of experiments into the vortex-induced cross-flow oscillations of a circular cylinder mounted elastically in a water channel. In these experiments, where the wake behind the cylinder is fully laminar, they captured the 'lock-in' phenomenon over the Reynolds number range 106–126.

We interpreted the experiments in terms of a finite element model employing the analytical conditions shown in Figure 6 and the mesh deformation pattern shown in Figure 7. To simplify this problem, the structure is idealized as a rigid body supported by elastic springs in the Y-direction. The region of deformable finite elements is restricted to the square region around the cylinder in order to reduce the computational load.

The resonance of the cylinder vibration used for the calculation is set up according to the experiment. The parameters of the experimental conditions are given in Table I and Figure 6.

Using these experimental results as the calculational conditions, we performed a series of computations on the vortex-excited vibrations of the cylinder at $Re = 90$, 100, 110, 120, 130 and 140. Figure 8 shows the time histories of the non-dimensional cylinder displacement, lift coefficient and drag coefficient at $Re = 90$, 110 and 130 (each time history represents 4 s of real time) after each flow has reached a periodic state. At $Re = 90$, which is below the 'lock-in' regime of the experiment, the oscillation amplitude is small and modulated or 'beating' because of the difference between the vortex-shedding frequency and the natural cylinder frequency. From this flow at $Re = 90$ we increased the upstream velocity to $Re = 100$ until we obtained the regular periodic flow of Figure 8(b). At $Re = 100$, since the vortex-shedding frequency coincides with the natural frequency of the cylinder–spring

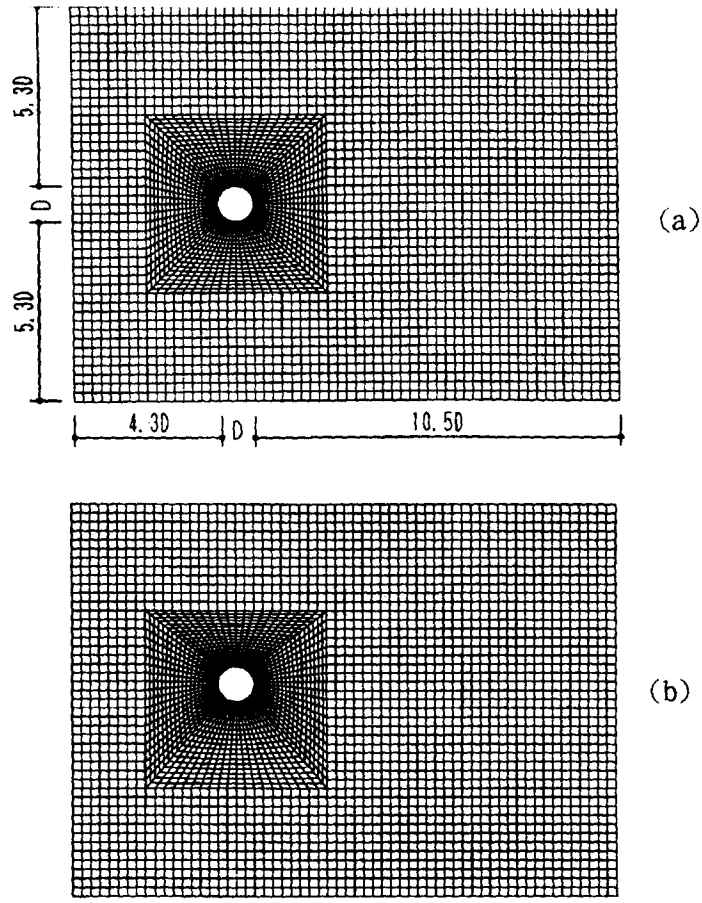

Figure 7. Finite element meshes: (a) undeformed mesh configuration; (b) deformed mesh configuration

system, f_n, the oscillation amplitude increases markedly. When we increased the upstream velocity to $Re = 120$, the vortex-shedding frequency remained at f_n. Finally, when we increased the upstream velocity to $Re = 130$, which is above the 'lock-in' regime of the experiment, the oscillation amplitude gradually decreased and the lift coefficient was 'beating' as in Figure 8(c). These features in the present computations are quite similar to those observed in the experiments on 'lock-in'.

Figure 9 summarizes the present computational results as well as the experimental data[1] and the calculational results of Nomura[13] for comparison. Using the present method, although the 'lock-in' phenomenon appears a little earlier than in the experiment, the f/f_n pattern agrees well with the experiment and the oscillation amplitudes are very close quantitatively to those of the experiment. In Nomura's[13] calculation, although the 'lock-in' range is a little narrow, the vortex-shedding frequencies coincide well with the expermental results, but the oscillation amplitudes are approximately half those

Table I. Parameters of reported experimental conditions[1]

St	0·1988	0·1789	0·1627	0·1491	0·1376	0·1278
Re	90	100	110	120	130	140
U(cm s^{-1})	5·646	6·274	6·901	7·529	8·156	8·783

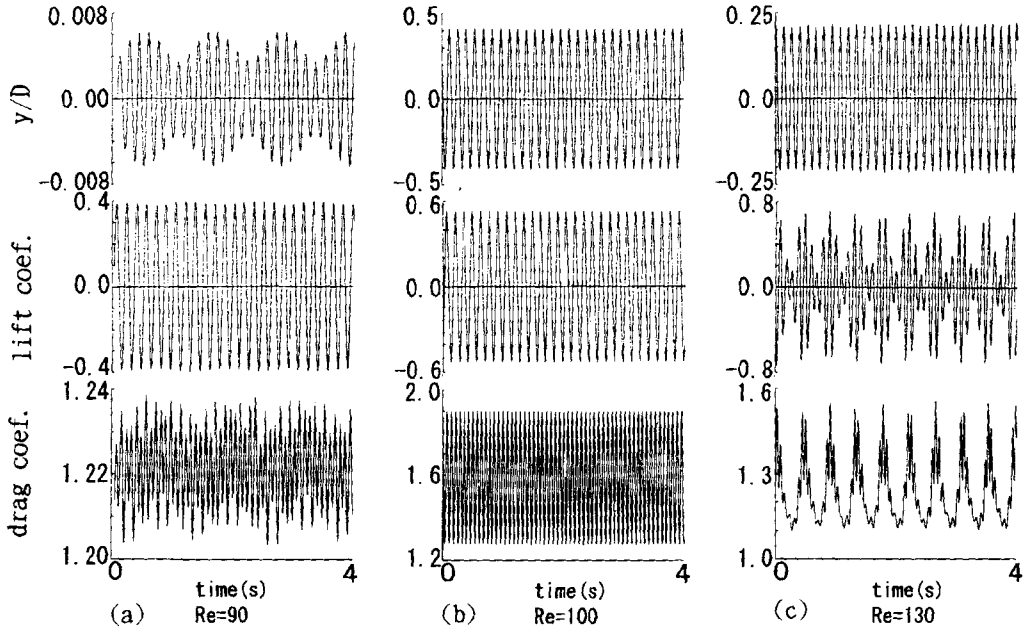

Figure 8. Histories of non-dimensional cylinder displacement and lift and drag coefficients

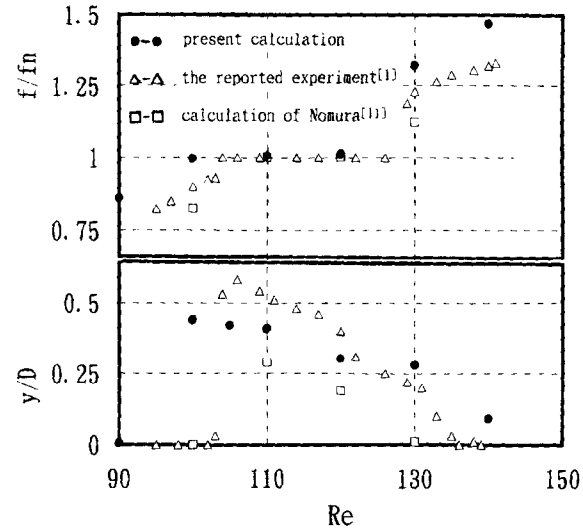

Figure 9. Comparison of oscillation amplitude and vortex-shedding frequency

of the experiment. In terms of the comparison of oscillation amplitudes the present method gives results closer to the experimental data.

5. CONCLUDING REMARKS

The problem of large-amplitude vortex-induced oscillations of a cylinder was solved stably and successfully by the present method, which employs the ALE formulation for the partial flow domain. The 'lock-in' phenomenon was captured quantitatively and agreed well with Anagnostopoulos and Bearman's[1] experiment. In actuality, high-Reynolds-number flow and turbulence models account for most of the phenomena in wind engineering. How to apply the present method to describe these phenomena is our future task.

REFERENCES

1. P. Anagnostopoulos and P. W. Bearman, 'Response characteristics of vortex-excited cylinder at low Reynolds numbers', *J. Fluids Struct.*, **6**, 39–50 (1992).
2. T. Belytschko and J. M. Kennedy, 'Computer models for sunassemly simulation', *Nucl. Eng. Design*, **49**, 17–38 (1978).
3. J. Donea, P. Fasoli-Stella and S. Ginliani, 'Lagrangian and Eulerian finite element techniques for transient fluid–structure interaction problems', *Trans. 4th SMiRT Conf.*, San Francisco, CA, 1977, Paper B1/2.
4. T. J. R. Hughes, W. K. Liu and T. K. Zimmermann, 'Lagrangian–Eulerian finite element formulation for incompressible viscous flows', *Comput. Methods Appl. Mech. Eng.*, **29**, 329–349 (1981).
5. W. K. Liu, H. Chang, J. S. Chen and T. Belytschko, 'Arbitrary Lagrangian–Eulerian Petrov-Galerkin finite elements for nonlinear continua', *Comput. Methods Appl. Mech. Eng.*, 259–310 (1988).
6. B. Ramaswamy and M. Kawahara, 'Arbitrary Lagrangian–Eulerian finite element method for unsteady, convective, incompressible viscous free surface flow', *Int. j. numer. methods fluids*, **7**, 1053–1075 (1987).
7. C. W. Hirt, A. A. Amsden and J. L. Cook, 'An arbitrary Lagrangian–Eulerian computing method for all flow speeds', *J. Comput. Phys.*, **14**, 227–253 (1974).
8. S. Mittal and T. E. Tezduyar, 'A finite element study of incompressible flows past oscillating cylinders and airfoils', *Int. j. numer. methods fluids*, **15**, 1073–1118 (1992).
9. A. Huerta and W. K. Liu, 'Viscous flow with large free surface motion', *Comput. Methods Appl. Mech. Eng.*, **69**, 277–324 (1988).
10. M. Shimura and M. Kawahara, 'Two dimensional finite element flow analysis using the velocity correction method', *Proc. JSCE*, (398), 255–263 (1988).
11. M. Shimura and O. C. Zienkiewicz, 'Interaction analysis between structure and fluid flow using the direct Laplacian method', *Proc. 4th Int. Conf. on Computer Applications in Civil and Building Engineering*, Tokyo, 1991, pp. 267–274.
12. T. Nomura and T. J. R. Hughes, 'An arbitrary Lagrangian–Eulerian finite element method for interaction of fluid and a rigid body', *Comput. Methods Appl. Mech. Eng.*, **59**, 115–138 (1992).
13. T. Nomura, 'Finite element analysis of vortex-induced vibrations of bluff cylinders', *J. Wind Eng. Ind. Aerodyn.*, **46–47**, 587–594 (1993).
14. A. Sekine and M. Shimura, 'Interaction analysis between structure and flow for wind engineering', *J. Wind Eng. Ind. Aerodyn.*, **46–47**, 595–604 (1993).